



# The interaction of hydrodynamic shocks with self-gravitating clouds

S. A. E. G. Falle,<sup>1</sup>★ B. Vaidya<sup>2</sup> and T. W. Hartquist<sup>3</sup>

<sup>1</sup>Department of Applied Mathematics, University of Leeds, Leeds LS2 9JT, UK

<sup>2</sup>Dipartimento di Fisica, University of Torino, Via Pietro Giuria, 1, I-10125 Torino, Italy

<sup>3</sup>School of Physics and Astronomy, University of Leeds, Leeds LS2 9JT, UK

Accepted 2016 October 27. Received 2016 October 27; in original form 2016 September 5

## ABSTRACT

We describe the results of 3D simulations of the interaction of hydrodynamic shocks with Bonnor–Ebert spheres performed with an adaptive mesh refinement code. The calculations are isothermal and the clouds are embedded in a medium in which the sound speed is either 4 or 10 times that in the cloud. The strengths of the shocks are such that they induce gravitational collapse in some cases and not in others, and we derive a simple estimate for the shock strength required for this to occur. These results are relevant to dense cores and Bok globules in star-forming regions subjected to shocks produced by stellar feedback.

**Key words:** hydrodynamics – shock waves – stars: formation.

## 1 INTRODUCTION

It has long been recognized that the triggering of gravitational collapse by shocks could be important in star formation. For example, Elmegreen & Lada (1977) showed that the dense layer between the shock and an ionization front can be gravitationally unstable, and Cameron & Truran (1977) suggested that a supernova-induced birth of the Solar system could account for the presence of short-lived radioisotopes (SLRIs) in meteorites. There is also considerable observational evidence for star formation triggered by supernovae, ionization fronts, protostellar outflows and other shocks in the interstellar medium (e.g. Preibisch et al. 2002; Yokogawa et al. 2003; Lee & Chen 2009; Snider et al. 2009).

There have been a considerable number of simulations of shocks interacting with gravitationally bound clouds (see e.g. Boss 1995; Foster & Boss 1996, 1997; Boss & Foster 1998; Vanhala & Cameron 1998; Vanhala & Boss 2002; Boss et al. 2008; Leão et al. 2009; Boss & Keiser 2010, 2012; Boss et al. 2010; Gritschneider et al. 2012; Boss & Keiser 2013; Li, Frank & Blackman 2014). These do, indeed, show that shock waves can trigger gravitational collapse, as long as the radiative cooling time is sufficiently short.

In a previous paper (Vaidya, Hartquist & Falle 2013), we considered the interaction of isothermal, plane-parallel shocks with magnetically subcritical clouds. Although gravitational collapse cannot occur in such clouds in the absence of ambipolar diffusion, we found that shocks with Alfvénic Mach numbers of 2 could produce a temporary increase in the density by a factor of  $10^3$ . This is due to a combination of shock focusing and magnetohydrodynamic (MHD) effects rather than gravitational collapse.

In this paper, we will consider the purely hydrodynamic version of this problem, that of an isothermal shock interacting with an isothermal Bonnor–Ebert sphere. This is exactly the same as that considered by Li et al. (2014), but they considered only a small number of cases, whereas our purpose is to derive a simple expression for the shock strength required to induce gravitational collapse. The astrophysical application which we have in mind is that of the dense, quasi-stationary cores found in star-forming regions, which in many cases appear to be close to Bonnor–Ebert spheres (e.g. Schnee et al. 2010). These are presumably gravitationally stable, but their collapse could be triggered by shocks due to stellar winds and jets, ionization fronts and supernovae.

We will also briefly consider the effect of self-gravity on Kelvin–Helmholtz and Richtmyer–Meshkov instabilities since these may be important for cloud destruction and mixing of SLRIs into gas, which will form a protoplanetary system (see e.g. Boss & Keiser 2013).

Section 2 describes the numerical method and initial and boundary conditions. The general evolution of the clouds is discussed in Section 3, and a comparison of the development of non-gravitational instabilities in models with and without self-gravity is presented in Section 4. Section 5 concludes this paper.

## 2 NUMERICAL METHOD AND INITIAL CONDITIONS

### 2.1 Numerical code

The calculations were performed with the hierarchical adaptive mesh refinement (AMR) code MG (Falle, Hubber & Goodwin 2013). This solves the equations of hydrodynamics using a second-order upwind scheme described in Falle (1991). A hierarchy of  $n$  grids levels,  $G_0 \dots G_{n-1}$ , is used, and the mesh spacing for  $G_n$  is  $\Delta x/2^n$ , where  $\Delta x$  is the cell size for the coarsest level,  $G_0$ .  $G_0$  and  $G_1$  cover the entire domain, but finer grids need not do so. Refinement is

\* E-mail: S.A.E.G.Falle@leeds.ac.uk

**Table 1.** Simulation parameters. Here,  $\rho_c$  is the central density in the equilibrium Bonnor–Ebert sphere,  $\rho_{\max}$  is the maximum density attained,  $M_s$  is the incident shock Mach number,  $M_1$  is the shock Mach number for which the post-shock pressure is equal to 1.4 and  $M_2$  is the Mach number for which the pressure behind the bow shock is equal to 1.4.

State	$\rho_c$	$P_e$	$c_e$	$M_1$	$M_2$	$M_s$	$\rho_{\max}/\rho_c$	Maximum resolution	Behaviour
1	0.37	0.2	10.0	2.65	1.91	2.1	$1.74 \times 10^3$	$1280^3$	Rebound
						2.2	$2.88 \times 10^3$	$1280^3$	Rebound
						2.3	–	$2560^3$	Collapse
2	0.37	0.2	4.0	2.65	1.91	2.0	$2.88 \times 10^2$	$1280^3$	Rebound
						2.1	$5.55 \times 10^2$	$1280^3$	Rebound
						2.2	–	$1280^3$	Collapse
3	1.09	0.45	4.0	1.76	1.66	1.6	91.6	$1280^3$	Rebound
						1.7	–	$1280^3$	Collapse
4	2.16	0.7	4.0	1.41		1.4	72.4	$1280^3$	Rebound
						1.5	–	$1280^3$	Collapse
5	3.9	0.95	4.0	1.21		1.2	20.6	$1280^3$	Rebound
						1.3	–	$1280^3$	Collapse

on a cell-by-cell basis and is controlled by error estimates based on the difference between solutions on different grids; that is, the difference between the solutions on  $G_{n-1}$  and  $G_n$  determines refinement to  $G_{n+1}$ . Self-gravity is computed using a full approximation multigrid to solve the Poisson equation.

## 2.2 Domain and grids

Although the problem is axisymmetric, the calculations were performed on a 3D Cartesian grid. This saves us the trouble of writing an axisymmetric Poisson solver and has the merit that it allows for non-axisymmetric instabilities, which are sufficiently strong to be triggered by rounding error. The domain is  $-2 \leq x \leq 2$ ,  $-2 \leq y \leq 2$  and  $-2 \leq z \leq 2$ , with the centre of the cloud initially at the origin. Initially, six grids were used with a resolution of  $10^3$  on  $G_0$ , which gives an effective maximum resolution of  $320^3$ . Note that  $G_0$  needs to be coarse in order to ensure fast convergence of the multigrid Poisson solver. This resolution is more than adequate for the equilibrium state but is not sufficient to resolve the high-density region which is produced by the shock interaction. However, the code has the ability to resolve such regions by increasing the number of refinement levels during the course of the calculation (see Table 1 for the effective resolution in each run).

Truelove et al. (1997) have pointed out that, in calculations involving gravitational collapse, one needs to resolve the Jeans length

$$\lambda_J = \left( \frac{\pi c^2}{G \rho} \right)^{1/2}, \quad (1)$$

where  $c$  is the sound speed and  $\rho$  is the density. They suggest that the mesh spacing needs to be  $\simeq 0.25\lambda_J$  to avoid artificial fragmentation when a dense region moves from a fine to a coarse grid. This is not a situation which occurs in these calculations, but it is nevertheless useful to compare the mesh spacing with  $\lambda_J$ .

The highest density and hence the smallest Jeans length in a non-collapsing case occurs in the State 1  $M_s = 2.2$  calculation and this gives  $\lambda_J = 0.033$ . The mesh spacing in this case is  $\Delta x = 0.0031$ , so the Jeans length is comfortably resolved. It is even better resolved in the other non-collapsing cases. In the collapsing cases, the calculation is stopped before the Jeans length becomes unresolved, by which time it is clear that the collapse is unstoppable.

## 2.3 Initial conditions

We first compute the collapse of an initially uniform, non-rotating, isothermal, spherical cloud to a stable hydrostatic equilibrium state. The cloud has a sound speed  $c_c$  and is embedded in a warmer uniform medium with sound speed  $c_e$  and pressure  $P_e$ . The cloud material is tracked with an advected scalar  $\alpha$ , which is unity in the cloud and zero in the surroundings. The sound speed  $c$  is given by

$$c^2 = \alpha c_c^2 + (1 - \alpha)c_e^2. \quad (2)$$

The scalar is also used to turn off gravity in the external medium.

We use units in which  $c_c = 1$ , the gravitation constant  $G = 1$  and the mass of the cloud  $m = 1$ . In these units, the maximum external pressure which can be supported by a stable Bonner–Ebert sphere is  $P_{\max} \simeq 1.4$  (Bonnor 1956). We consider four stable states with external pressures  $P_{\text{ext}} = 0.95, 0.7, 0.45, 0.2$  (see Table 1). These states were generated by starting with a uniform density cloud with  $\rho = 1$ . The initial radius is then fixed by the requirement that the mass of the cloud is unity.

This initial state was then allowed to collapse until it reached equilibrium. As noted by Boss et al. (2010), a cloud formed in this way oscillates about the Bonner–Ebert state for some time. This was prevented by imposing a drag force of the form

$$\mathbf{F}_d = -A\rho\mathbf{v}, \quad (3)$$

where  $A$  is a suitable coefficient and  $\mathbf{v}$  is the velocity. The drag force is switched off once the cloud has become static.

## 3 SHOCK INTERACTION

Once an equilibrium Bonner–Ebert sphere has been obtained, a planar isothermal shock with Mach number  $M_s$  moving in the negative  $x$  direction is introduced near the cloud. The density and velocity at  $x = 2$  are fixed at the values given by the Rankine–Hugoniot jump conditions for a shock with isothermal Mach number  $M_s$  propagating into the medium surrounding the cloud. We considered a number of different cases with different external pressures and sound speeds, as summarized in Table 1.

The only dimensionless parameters are the incident shock Mach number,  $M_s$ , the ratio of the initial external pressure,  $P_e$ , to the maximum pressure of a stable Bonner–Ebert sphere,  $P_{\max}$ , and the ratio of the sound speeds,  $c_c$  and  $c_e$ . In the case considered by Li et al. (2014), the cloud had a mass of  $1 M_\odot$ , a temperature of 10 K,

and a radius of 0.058 pc in an external medium at 1000 K. This gives the same ratio of sound speeds as in our State 1 (see Table 1), but their initial external pressure was  $0.914 P_{\max}$ , so that their cloud was closer to collapse than any of our cases. It is therefore not surprising that they find that a shock with a Mach number of 1.5 induces collapse. One could also apply our results to other cases, such as Bok globules with masses in the range of  $10\text{--}100 M_{\odot}$ , which are known to be associated with young stars (Yun & Clemens 1990). It is useful to define an incident shock crossing-time by

$$t_c = \frac{R}{c_e M_s}, \quad (4)$$

where  $R$  is the radius of the equilibrium cloud, which is the time-scale on which the flow outside the cloud becomes quasi-steady. The other relevant time-scale is an estimate of the time it takes for the transmitted shock in the cloud to reach the centre, which Klein, McKee & Colella (1994) call the ‘cloud-crushing time’. They use

$$t_{cc} = t_c \frac{\rho_{\text{cloud}}}{\rho_e}, \quad (5)$$

where  $\rho_{\text{cloud}}$  is the (uniform) density of the cloud. Li et al. (2014) set  $\rho_{\text{cloud}} = \rho_c$ , where  $\rho_c$  is the central density. We shall see later that this is not always a good estimate of the time at which the maximum density in the cloud begins to increase.

Fig. 1 shows the density and velocity vectors in the  $z = 0$  plane at different times for State 1,  $M_s = 2.2$  simulation. In the top left-hand panel ( $t = 3.359 t_c$ ), the incident shock has passed the cloud, formed a quasi-steady bow shock and is driving a transmitted shock into the cloud. In the middle left-hand panel ( $t = 11.292 t_c$ ), the transmitted shock has reached the centre of the cloud and created a high-density region. The middle right-hand panel is at the time at which the density is maximum ( $t = 14.662 t_c$ ), and in the bottom left-hand panel ( $t = 17.426 t_c$ ), the cloud is re-expanding. The bottom right-hand panel ( $t = 23.138 t_c$ ) shows a blow-up of the expanding cloud with velocity arrows in the rest frame of the densest region.

The convergence of the transmitted shock at the centre is shown in more detail in Fig. 2. Here, we can see that a jet is produced in much the same way as in a shaped charge (Birkhoff et al. 1948). This jet interacts with other parts of the cloud to produce a secondary high-density region (bottom left-hand panel). The maximum density is much larger than that behind the initial transmitted shock; it is clear that flow convergence has a significant effect. There are some similarities with the magnetic case described in Vaidya et al. (2013), but the latter is more complicated due to the dynamic effects of the magnetic field. However, despite the high density, there is no collapse in this case because the high-density region is too small to be gravitationally unstable.

Fig. 3 shows what happens for State 1 in the  $M_s = 2.3$  case, which does collapse. The flow evolves in much the same way, except that the high-density region collapses in this case.

Table 1 shows that the Mach number of a shock which induces collapse does not decrease by much when the external sound speed is reduced to 4 (State 2), and in fact, the flow is very similar to that for State 1. This is not too surprising since in both cases the density contrast is large enough for the evolution of the flow around the cloud to be quasi-steady. The values of the maximum density obtained for different simulations are listed in Table 1. One can see from Fig. 7 that the cloud bounces even in those cases in which it subsequently undergoes collapse.

It would obviously be useful to have a rule of thumb to determine the strength of the shock required for collapse. Consider a plane isothermal shock with speed  $s$  in a medium at rest with sound speed

$c$ , density  $\rho_e$  and pressure  $P_e = c^2 \rho_e$ . The density and velocity behind the shock are

$$\rho_1 = \rho_e M^2 \quad (6)$$

and

$$\mathbf{v}_1 = s \left( 1 - \frac{1}{M^2} \right). \quad (7)$$

The pressure is therefore

$$P_1 = M^2 c^2 \rho_e = M^2 P_e. \quad (8)$$

The most obvious estimate of the critical Mach number for collapse is to set  $P_1 = P_{\max} = 1.4$ , the maximum external pressure that the cloud can support, which gives the Mach number  $M_1$  shown in Table 1. One can see that this works quite well for the cases with a larger initial external pressure (States 4 and 5) but is an overestimate for the lower initial pressures (States 1, 2 and 3). One might suppose that this is because shock convergence induces larger pressures than that behind the incident shock.

However, as we have already pointed out, the flow around the cloud evolves to become approximately quasi-steady, so the relevant pressure should really be that in a steady flow around the cloud. In such a flow, the maximum pressure is that behind a stationary shock, whose upstream state is that behind the incident shock, i.e.  $v = v_1$  and  $\rho = \rho_1$ . The post-shock density and pressure are therefore

$$\rho_2 = \rho_1 \left( \frac{v_1}{c} \right)^2 = \rho_e M^4 \left( 1 - \frac{1}{M^2} \right)^2, \quad (9)$$

$$P_2 = \frac{\rho_2}{\rho_e} P_e = M^4 \left( 1 - \frac{1}{M^2} \right)^2 P_e. \quad (10)$$

Setting  $P_2 = P_{\max} = 1.4$  gives the Mach number  $M_2$  shown in Table 1. This works very well for State 3 and is somewhat better than  $M_1$  for States 1 and 2. Note that  $M_2$  is not defined for States 4 and 5 since it would imply a subsonic flow behind the incident shock. In fact, the State 4 and 5 simulations are somewhat dubious since the flow is subsonic behind the weakest incident shock which induces collapse, which is incompatible with our imposition of the post-shock state at the right-hand  $x$ -boundary. Nevertheless,  $M_2$  significantly underestimates the Mach number required for collapse for States 1 and 2. Fig. 4 depicts that for State 1, only a fairly small part of the surface of the cloud experiences a pressure greater than  $P_{\max}$ , and the same is true for State 2. Clearly shock convergence helps, but it does not produce a large enough high-density region for collapse, unless the incident Mach number is somewhat higher than  $M_2$ .

One can see from Fig. 5 that almost the whole of the surface of the cloud experiences a pressure greater than  $P_{\max}$  in the subsonic flow behind the incident shock for State 5, and this is also true for State 4. This is why  $M_1$  is a good estimate for these cases. However, as we have already pointed out, the calculations are not entirely trustworthy for these cases, and even if they were, clouds so close to collapse would not be of much interest.

Note that neither  $M_1$  nor  $M_2$  depends on the initial density ratio between the cloud and its surroundings,  $c_c^2/c_e^2$ , since  $M_1$  depends simply on the pressure behind the incident shock and  $M_2$  on the pressure behind a quasi-steady bow shock. The critical value of  $M_s$  for collapse is also insensitive to the density ratio; it is very nearly the same for States 1 and 2. This is because the density ratio is large enough for the ‘cloud crushing time’ given by equation (5) to be significantly larger than the shock crossing time, given by equation (4). The flow outside the cloud is therefore approximately

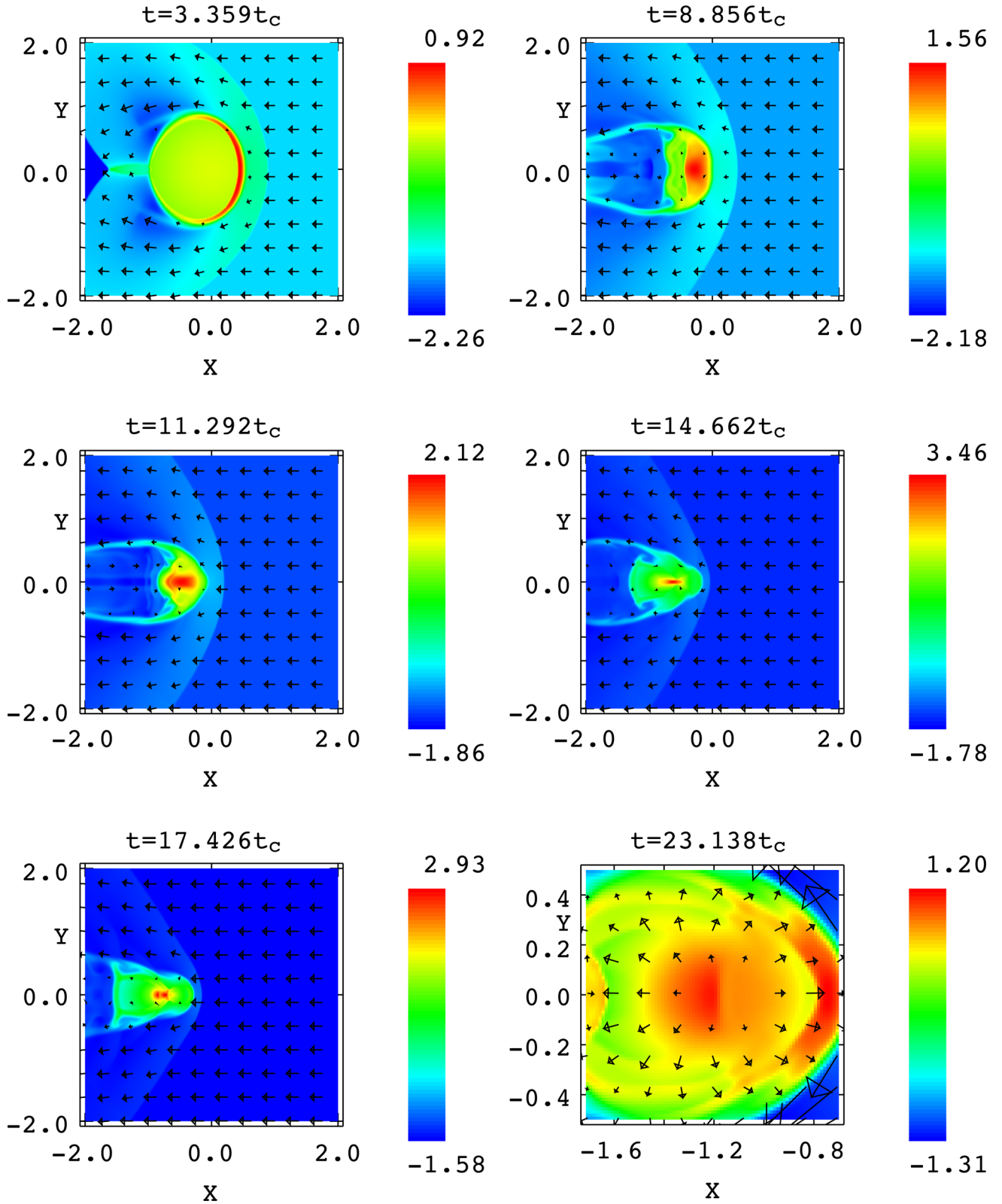


**Figure 1.** Logarithm of the ratio of the density to the central density in the equilibrium state, and velocity arrows in the  $z = 0$  plane for the State 1,  $M_s = 2.2$  simulation. The velocity arrows in the bottom right-hand panel are in the rest frame of the dense region.

quasi-steady by the time the transmitted shock reaches the centre of the cloud. This is true from Figs 6 and 7: The cloud density does not begin to increase significantly until  $t \simeq 10t_c$  for State 1 and  $t \simeq 5t_c$  for State 2. Note that the ‘cloud crushing time’ defined by

equation (5) gives a reasonable estimate of this time:  $t_{cc} = 13.6t_c$  for State 1 and  $t_{cc} = 5.4t_c$  for State 2. However, the estimate is not so good for State 5, for which  $t_{cc} = 8.1t_c$ , while the density begins to increase rapidly at  $t \simeq 2.5t_c$ . This is largely because this cloud is

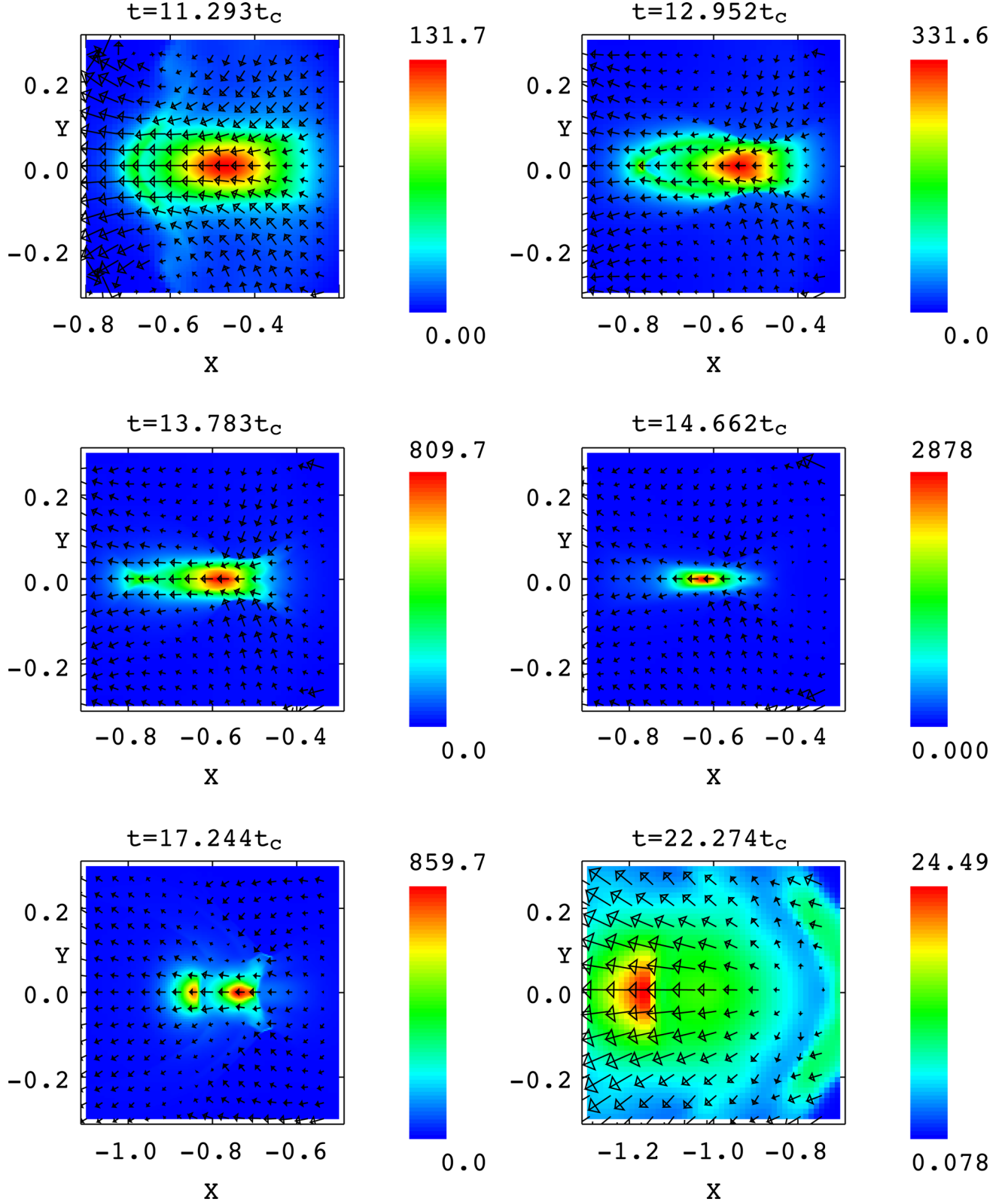


**Figure 2.** Detail of the shock convergence for the State 1,  $M_s = 2.2$  simulation. Same as Fig. 1 except that the density scale is linear and all the velocity arrows are in the initial rest frame of the cloud.

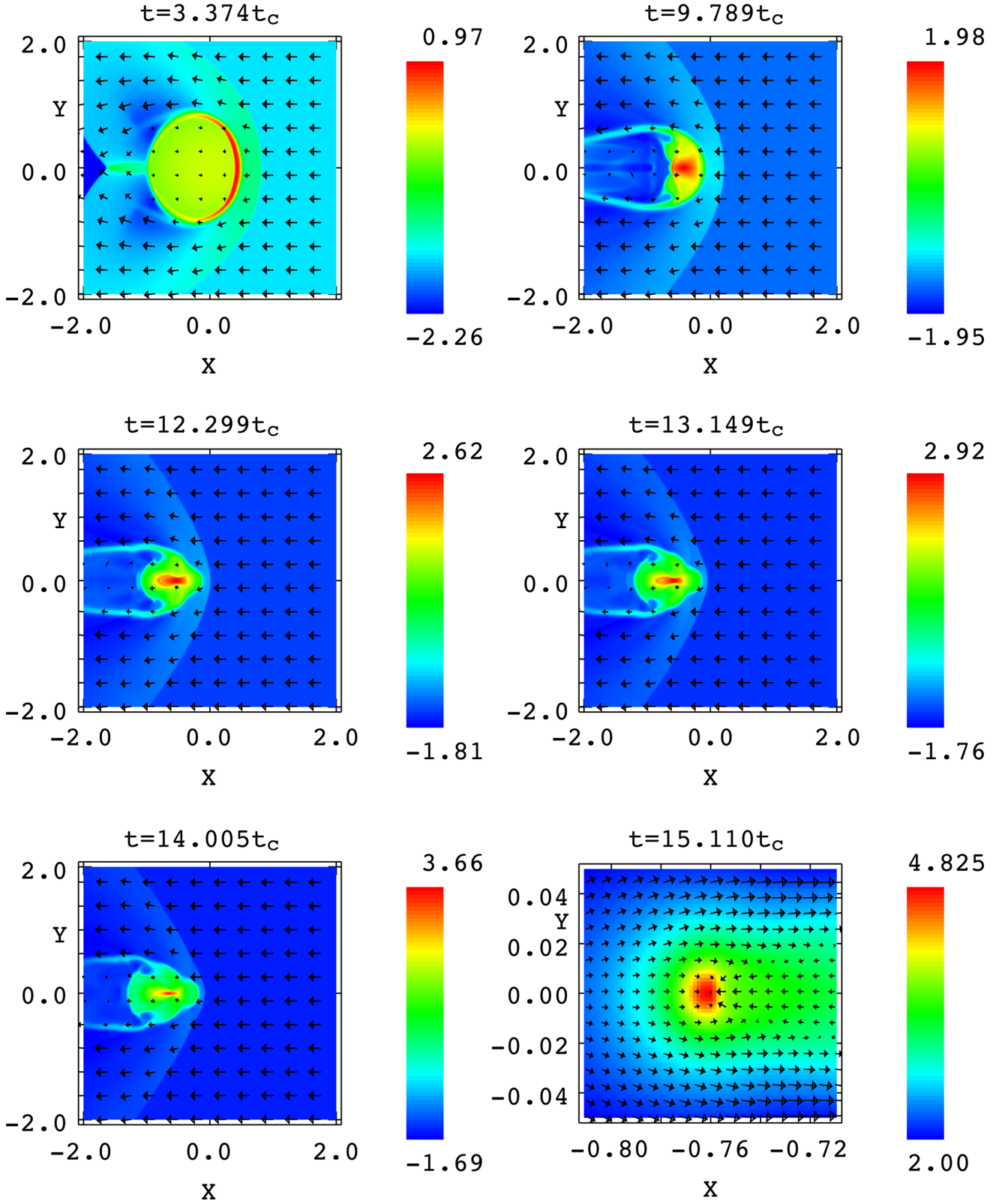


**Figure 3.** Logarithm of the ratio of the density to the central density in the equilibrium state and velocity arrows in the  $z = 0$  plane for the State 1,  $M_s = 2.3$  simulation. The velocity arrows in the bottom right-hand panel are in the rest frame of the dense region.

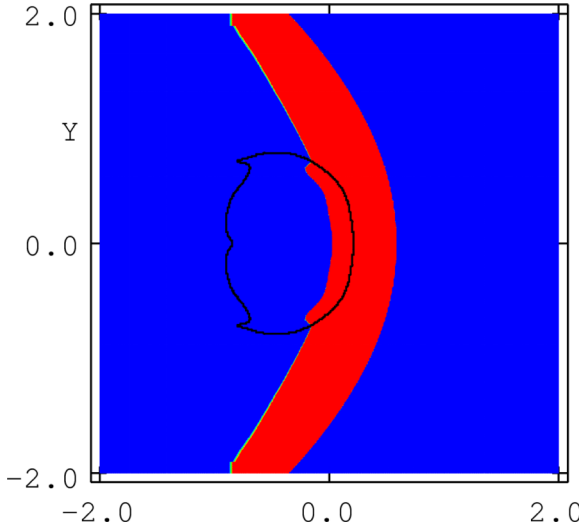


**Figure 4.** Red shows the region where the pressure is greater than  $P_{\max}$  for the State 1  $M_s = 2.3$  calculation at  $t = 5.49t_c$ . The boundary of the cloud is the black contour.

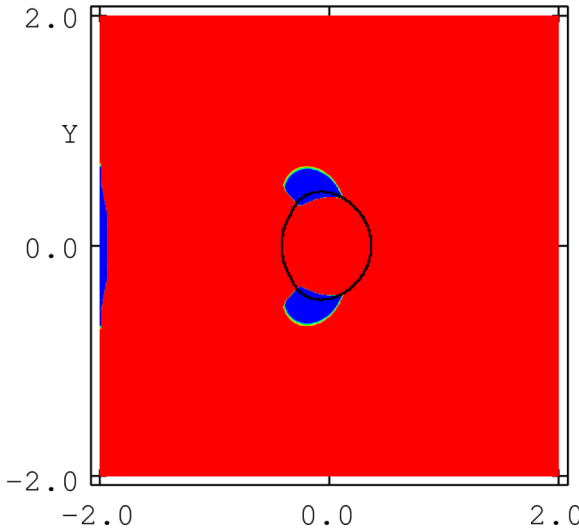


**Figure 5.** Red shows the region where the pressure is greater than  $P_{\max}$  for the State 5  $M_s = 1.3$  calculation at  $t = 4.82t_c$ . The boundary of the cloud is the black contour.

more centrally condensed, so that the speed of the transmitted shock in the outer parts of the cloud is larger than that used to estimate  $t_{cc}$ .

#### 4 HYDRODYNAMIC INSTABILITIES

There has recently been a considerable work on the possibility that the short-lived radio isotopes found in meteorites could have been injected into the solar nebula by instabilities during an interaction with a supernova shell (e.g. Boss & Keiser 2012; Li et al. 2014). Although it is not the main focus of this paper, it is worth looking at any instabilities which might occur.

One might expect self-gravity to have a stabilizing effect on instabilities at the cloud surface since it is Rayleigh–Taylor stable. The simulations described in the previous section do indeed show little evidence of either Kelvin–Helmholtz or Richtmyer–Meshkov instabilities at the cloud surface, but there is a weak non-axisymmetric Kelvin–Helmholtz instability in the wake. However, a stronger in-

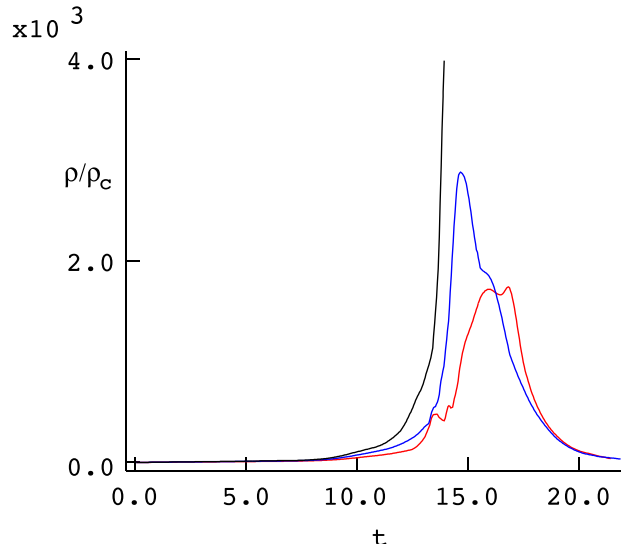


**Figure 6.** Ratio of the maximum density to the initial central density,  $\rho_c$ , for State 1 as functions of time.  $M_s = 2.1$  – red;  $M_s = 2.2$  – blue;  $M_s = 2.3$  – black (see Table 1).

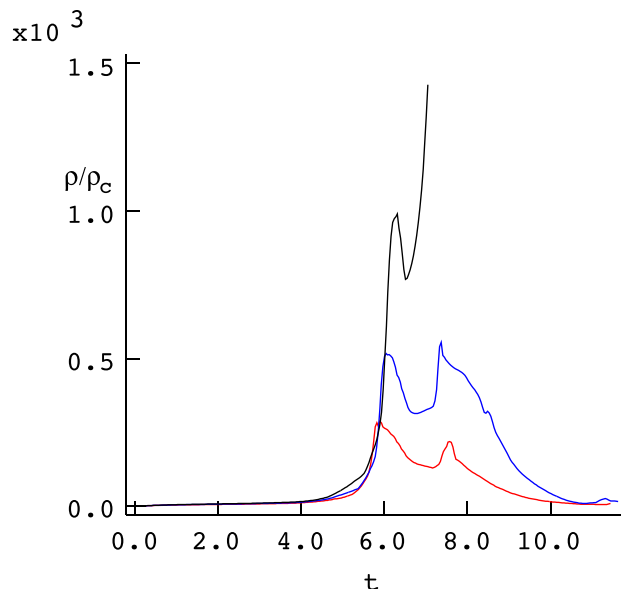


**Figure 7.** Ratio of the maximum density to the initial central density,  $\rho_c$ , for State 2 as functions of time.  $M_s = 2.0$  – red,  $M_s = 2.1$  – blue and  $M_s = 2.2$  – black (see Table 1).

cident shock does induce Richtmyer–Meshkov instabilities on the front surface of the cloud. Fig. 8 shows the density in the  $z = 0$  and  $x = 0.2$  planes for a State 1,  $M_s = 5$  simulation at a time at which the incident shock has just passed the cloud. A non-axisymmetric Richtmyer–Meshkov instability is clearly present and has not been suppressed by self-gravity. One can see from Fig. 9, which shows the cloud scalar, that the instability does lead to some mixing behind the shock in the cloud. However, this shock simply shreds the cloud without causing gravitational collapse. This is consistent with the results in Boss & Keiser (2012): If the shock is too weak, there is very little instability, whereas if it is too strong, it destroys the cloud.

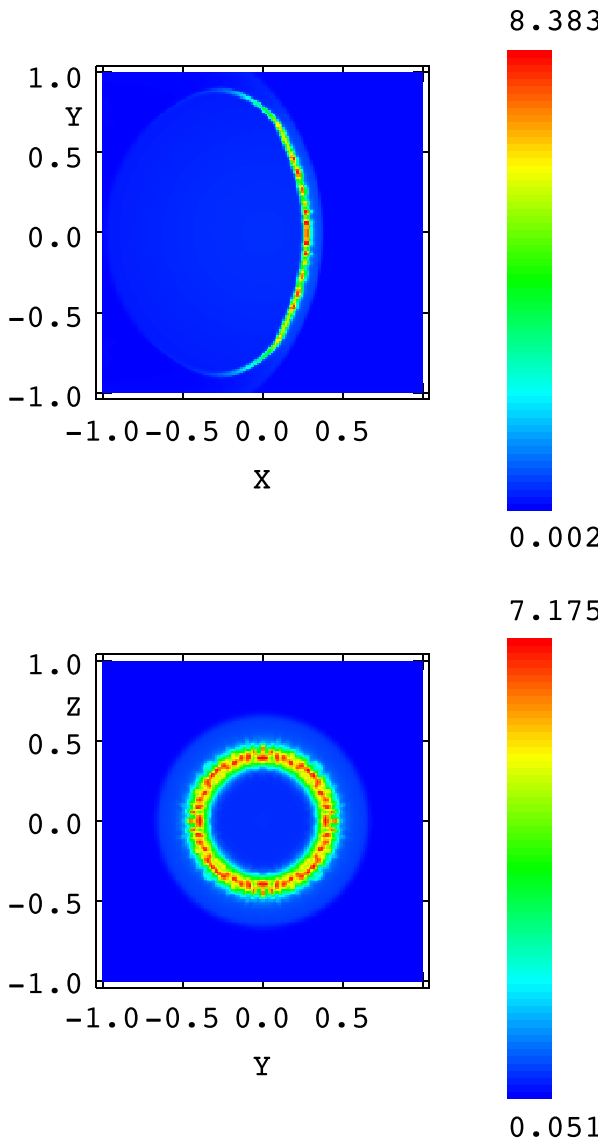


**Figure 8.** Density in the  $z = 0$  plane (top panel) and  $x = 0.2$  plane (bottom panel) for the State 1,  $M_s = 5.0$  simulation at  $t = 2.398t_c$ .

## 5 CONCLUSIONS

We have found that the minimum Mach number  $M_s$  of a shock which induces collapse in a previously stable self-gravitating cloud is not sensitive to the initial density ratio between the cloud and its surroundings, as long as it is sufficiently large. The minimum value of  $M_s$  lies between  $M_2$  and  $M_1$ , where for  $M_s = M_1$  the pressure behind the incident shock is equal to the maximum pressure,  $P_{\max}$ , which the cloud can sustain, whereas for  $M_s = M_2$ , the maximum pressure behind the bow shock is equal to  $P_{\max}$ . A shock with a smaller value of  $M_s$  will compress a cloud until a peak density is reached, after which the cloud expands, but gravity prevents it from being disrupted. Such an expansion phase can occur even if  $M_s$  is large enough for collapse, but in such cases, gravity eventually drives collapse.

As in our simulations of shock interactions with magnetically subcritical clouds (Vaidya et al. 2013), the simulations described above show that shock focusing is responsible for the large value of the peak density which is reached even in clouds which do not collapse.

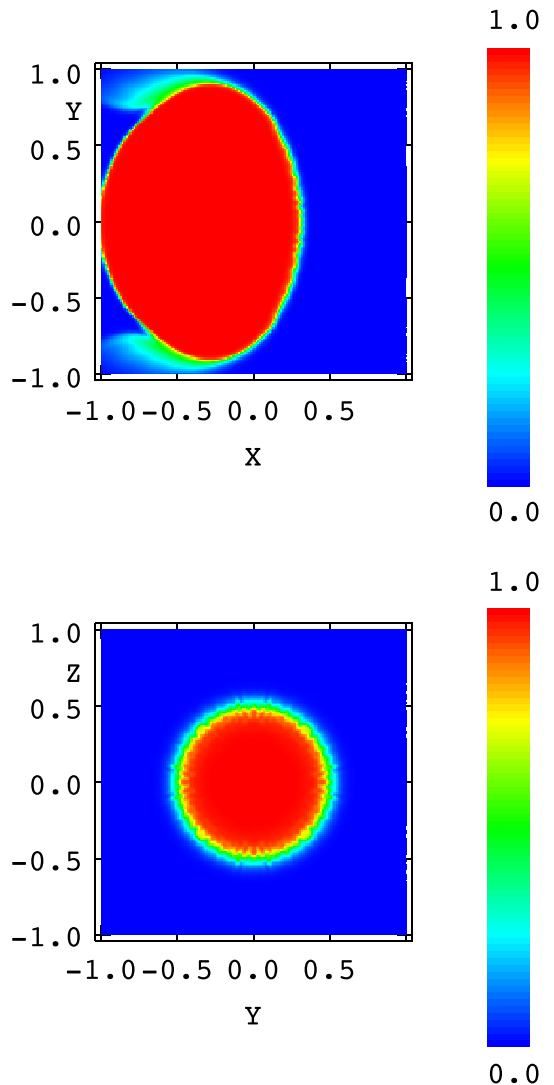


**Figure 9.** Cloud scalar in the  $z = 0$  plane (top panel) and  $x = 0.2$  plane (bottom panel) for the State 1,  $M_s = 5.0$  simulation at  $t = 2.398t_c$ .

## ACKNOWLEDGEMENTS

This work was supported by the Science & Technology Facilities Council (Research Grant ST/I001557/1). The calculations for this paper were performed on the DiRAC 1 Facility jointly funded by STFC, the Large Facilities Capital Fund of BIS and the University of Leeds. This facility is hosted and enabled through the ARC HPC resources and support team at the University of Leeds (A. Real, M. Dixon, M. Wallis, M. Callaghan and J. Leng), to whom we extend our grateful thanks. We thank an anonymous referee for helpful comments.

## REFERENCES

- Birkhoff G., MacDougall D., Pugh E., Taylor G., 1948, *J. Appl. Phys.*, 19, 563
- Bonnor W. B., 1956, *MNRAS*, 116, 351
- Boss A. P., 1995, *ApJ*, 439, 224
- Boss A. P., Foster P. N., 1998, *ApJ*, 494, L103
- Boss A. P., Keiser S. A., 2010, *ApJ*, 717, L1
- Boss A. P., Keiser S. A., 2012, *ApJ*, 756, L9
- Boss A. P., Keiser S. A., 2013, *ApJ*, 770, 51

- Boss A. P., Ipatov S. I., Keiser S. A., Myhill E. A., Vanhala H. A. T., 2008, *ApJ*, 686, L119
- Boss A. P., Keiser S. A., Ipatov S. I., Myhill E. A., Vanhala H. A. T., 2010, *ApJ*, 708, 1268
- Cameron A. G. W., Truran J. W., 1977, *Icarus*, 30, 447
- Elmegreen B. G., Lada C. J., 1977, *ApJ*, 214, 725
- Falle S. A. E. G., 1991, *MNRAS*, 250, 581
- Falle S. A. E. G., Hubber D. A., Goodwin S. P., 2013, *MNRAS*, 432, 711
- Foster P. N., Boss A. P., 1996, *ApJ*, 468, 784
- Foster P. N., Boss A. P., 1997, *ApJ*, 489, 346
- Gritschneider M., Lin D. N. C., Murray S. D., Yin Q.-Z., Gong M.-N., 2012, *ApJ*, 745, 22
- Klein R. I., McKee C. F., Colella P., 1994, *ApJ*, 420, 213
- Leão M. R. M., de Gouveia Dal Pino E. M., Falceta-Gonçalves D., Melioli C., Geraissate F. G., 2009, *MNRAS*, 394, 157
- Lee H.-T., Chen W. P., 2009, *ApJ*, 694, 1423
- Li S., Frank A., Blackman E. G., 2014, *MNRAS*, 444, 2884
- Preibisch T., Brown A. G. A., Bridges T., Günther E., Zinnecker H., 2002, *AJ*, 124, 404
- Schnee S., Enoch M., Johnstone D., Culverhouse T., Leitch E., Marrone D. P., Sargent A., 2010, *ApJ*, 718, 306
- Snider K. D., Hester J. J., Desch S. J., Healy K. R., Bally J., 2009, *ApJ*, 700, 506
- Truelove J. K., Klein R. I., McKee C. F., Holliman J. H., 1997, *ApJ*, 489, L179
- Vaidya B., Hartquist T. W., Falle S. A. E. G., 2013, *MNRAS*, 433, 1258
- Vanhala H. A. T., Boss A. P., 2002, *ApJ*, 575, 1144
- Vanhala H. A. T., Cameron A. G. W., 1998, *ApJ*, 508, 291
- Yokogawa S., Kitamura Y., Momose M., Kawabe R., 2003, *ApJ*, 595, 266
- Yun M. L., Clemens D. P., 1990, *ApJ*, 365, L73

This paper has been typeset from a *T<sub>E</sub>X/L<sup>A</sup>T<sub>E</sub>X* file prepared by the author.